Accepted Manuscript

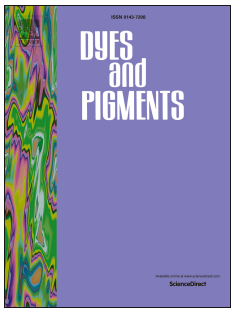

Efficient near-infrared emission based on donor-acceptor molecular architecture: The role of ancillary acceptor of cyanophenyl

Xiaohui Tang, Xiang-Long Li, Haichao Liu, Yu Gao, Yue Shen, Shitong Zhang, Ping Lu, Bing Yang, Shi-Jian Su, Yuguang Ma

PII: S0143-7208(17)31990-3

DOI: 10.1016/j.dyepig.2017.10.033

Reference: DYPI 6331

To appear in: *Dyes and Pigments*

Received Date: 20 September 2017

Revised Date: 20 October 2017

Accepted Date: 20 October 2017

Please cite this article as: Tang X, Li X-L, Liu H, Gao Y, Shen Y, Zhang S, Lu P, Yang B, Su S-J, Ma Y, Efficient near-infrared emission based on donor-acceptor molecular architecture: The role of ancillary acceptor of cyanophenyl, *Dyes and Pigments* (2017), doi: 10.1016/j.dyepig.2017.10.033.

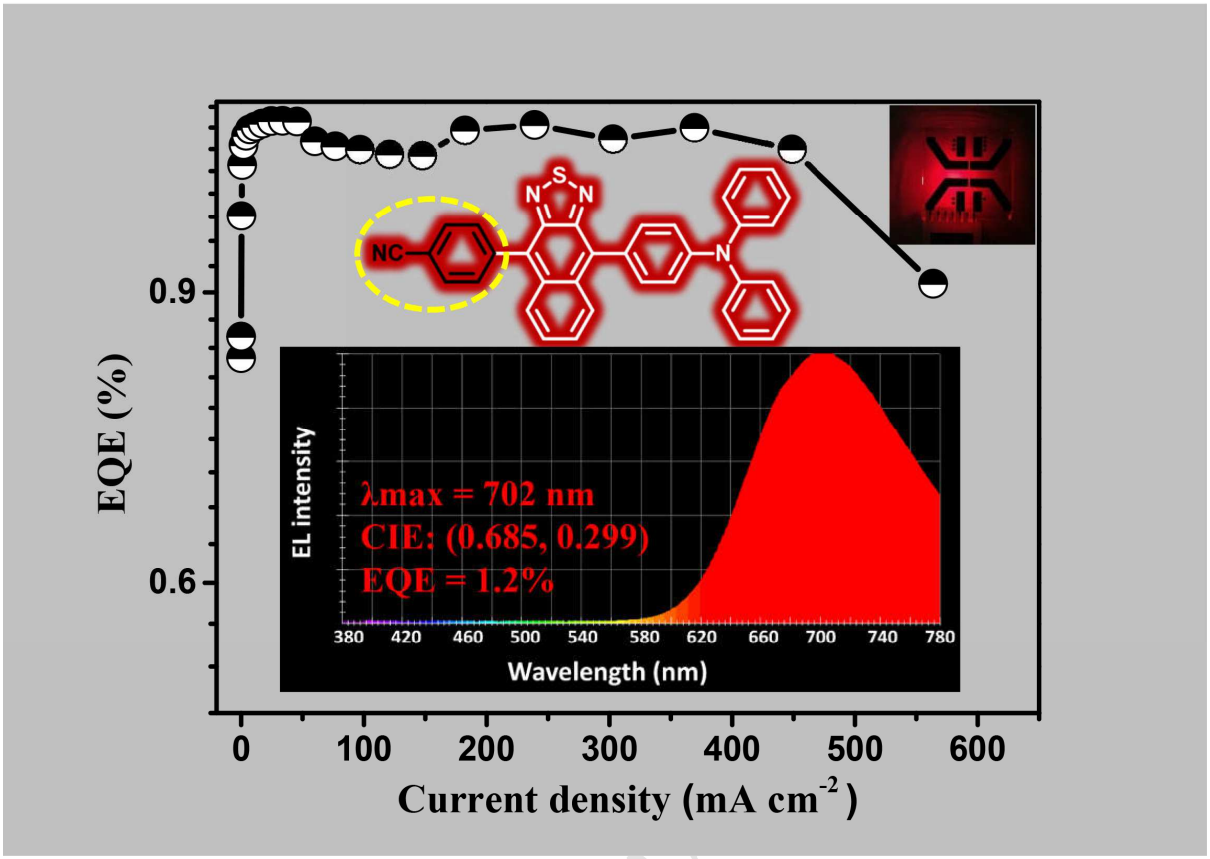

Efficient Near-infrared Emission Based on Donor-acceptor Molecular Architecture: the Role of Ancillary Acceptor of Cyanophenyl

Xiaohui Tang,[†a] Xiang-Long Li,[†b] Haichao Liu,[a] Yu Gao,[a] Yue Shen,[a] Shitong Zhang,[a] Ping Lu,[a] Bing Yang,[*a] Shi-Jian Su,[*b] and Yuguang Ma[b]

†: these authors contributed equally to this work

[a] *State Key Laboratory of Supramolecular Structure and Materials, Jilin University, Changchun, 130012, P. R. China.*

[b] *State Key Laboratory of Luminescent Materials and Devices, Institute of Polymer Optoelectronic Materials and Devices, South China University of Technology, Guangzhou, 510640, P. R. China.*

Corresponding Author

Bing Yang E-mail: yangbing@jlu.edu.cn

Shi-Jian Su E-mail: mssjsu@scut.edu.cn

Abstract: Herein, a new near-infrared (NIR) material, 4-(9-(4-(diphenylamino)phenyl)naphtho[2,3-*c*][1,2,5]thiadiazol-4-yl)benzonitrile (TPA-NZC), was designed and synthesized with the incorporation of an ancillary acceptor (cyanophenyl) into the donor-acceptor (D-A) molecular backbone of a red emitter TPA-NZP (4,9-diphenylnaphtho[2,3-*c*][1,2,5]thiadiazole). Compared with TPA-NZP, TPA-NZC exhibits an NIR emission (λ_{max} = 710 nm) with a large redshift, as well as a maintained photoluminescence efficiency (η_{PL}) of 17% in film. Moreover, the non-doped OLED based on TPA-NZC emitter exhibits an excellent NIR emission at 702 nm with a maximum EQE of 1.2%, while the doped device achieves a deep-red emission at 656 nm with a maximum EQE of 3.2%. This work further verifies the reliability of "hot exciton" and hybridized local and charge-transfer state (HLCT)

mechanism, as well as provides a strategy to design a narrow bandgap light-emitting material by introducing cyanophenyl as an ancillary acceptor in D-A systems.

Keywords: Near-infrared; hybridized local and charge-transfer state; hot exciton; cyanophenyl; OLEDs

1. Introduction

The development of near-infrared (NIR) light-emitting materials has aroused increasing interests, due to their important applications in many fields, such as organic light-emitting diodes (OLEDs), chemical sensors, biological imaging, information security, night-vision devices and so on [1-5]. However, NIR light-emitting materials with high photoluminescence (PL) efficiency (η_{PL}) are still relatively scarce compared to green and blue emitters. For high-efficiency NIR light-emitting materials, a great challenge is from the intrinsic limitation of the energy gap law, which tends to accelerate the non-radiative decay with a narrow energy gap, arising from the intensified vibrational overlap between excited state and ground state. Both phosphorescent (e.g. iridium and platinum metal-organic complexes) and fluorescent emitters are subject to this vibrational quenching by the energy gap law [6]. Generally, the phosphorescent metal complexes showed better PL and electroluminescence (EL) performance than fluorescent narrow-bandgap emitters, as a result of the enhanced spin-orbit coupling from heavy atom effect, enabling the full energy utilization of both singlet and triplet excitons [7-9]. More importantly, rational designed pure-organic fluorescent materials could also efficiently utilize the electro-triplet exciton, which is more promising in realizing superior comprehensive performance comparing to the metal-complexes, due to the advantages of structure richness, easy modification, low cost, good device stability and so on. Recently, the discovery of several new mechanisms, such as thermally-activated delayed fluorescence (TADF) [10-23], triplet-triplet annihilation (TTA) [24,25], hybridized local and charge-transfer state (HLCT) and “hot exciton” [26-34], greatly promotes the development of NIR OLEDs based on metal-free organic fluorescent D-A materials. The combination of “hot exciton” and HLCT shows the unique advantages in NIR fluorescent OLEDs. On the one hand, the HLCT state rationally combines the locally-excited (LE) state and charge-transfer

(CT) state, which is mainly responsible for high PL efficiency, especially for NIR narrow-bandgap materials. Molecules exhibiting HLCT states usually adopt the D-A structure, in favor of the balanced charge injection and charge transport [35]. On the other hand, "hot exciton" mechanism mainly contributes to high exciton utilization in NIR OLEDs. The typical characteristic of energy level structure includes a large energy gap between the first triplet state (T_1) and the second triplet (T_2) state, together with a small energy splitting between T_2 and singlet state (S_m, $m \geq 1$), which cooperatively promotes the singlet exciton proportion through reverse intersystem crossing (RISC) along "hot exciton" channel. The "hot exciton" mechanism can effectively suppress the accumulation of long-lifetime T_1 exciton, alleviating the triplet-triplet concentration quenching. Thus, it is very feasible to obtain highly efficient fluorescent NIR OLEDs with "hot exciton" and HLCT mechanism.

Naphtho[2,3-*c*][1,2,5]thiadiazole (NZ) group is commonly employed as an acceptor for narrow-bandgap D-A materials, due to its strong electron-withdrawing capability. Moreover, its unique energy level distribution accords with "hot exciton" characteristics [36]. It has been reported that the excited state properties of NZ group is modulated by introducing a donor group, achieving "hot exciton" and HLCT simultaneously [37-39]. Cyanophenyl is a commonly-used auxochrome in the field of optoelectronics, which shows both electron-withdrawing and conjugation effect [40-43]. In this contribution, cyanophenyl as an ancillary acceptor is attached to NZ group for a highly efficient NIR material, 4-(9-(4-(diphenylamino)phenyl)naphtho[2,3-*c*][1,2,5]thiadiazol-4-yl)benzonitrile (TPA-NZC), in which triphenylamine (TPA) acts as donor and 4-(naphtho[2,3-*c*][1,2,5]thiadiazol-4-yl)-*N*,*N*-diphenylaniline (NZC) serving as a strong acceptor. Both experimental and theoretical results demonstrate the "hot exciton" and HLCT characteristic of TPA-NZC molecule. The non-doped NIR OLEDs based on TPA-NZC emitter achieves a maximum external quantum efficiency (EQE) of 1.2% with an EL wavelength at 702 nm, while the doped device obtains a maximum EQE of 3.2% with a deep-red EL at 656 nm.

2. Experimental section

2.1. General: The ^{1}H and ^{13}C NMR spectra were recorded on AVANCE 500

spectrometers at 500 MHz and 125 MHz respectively, utilizing tetramethylsilane (TMS) as a standard. The compounds were characterized by a FlashEA 1112, CHNS-O elemental analysis instrument. The MALDI-TOF-MS mass spectra were recorded using an AXIMA-CFRTM plus instrument. The Fourier transform infrared spectroscopy FTIR spectra of TPA-NZC and M2 were recorded as KBr disks at room temperature by a Bruker VERTEX 80V FT-IR spectrometer, equipped with a DTGS detector at a resolution of 4 cm^{-1}.

2.2. Photophysical measurements: UV-vis absorption spectra were recorded on a UV-3100 spectrophotometer. Fluorescence measurements were carried out with a FLS980 Spectrometer. The NIR measurement was performed with InGaAs PDA NIR detector. The PL efficiencies in solvents are measured with a UV-3100 and FLS980, relative to Rhodamine B. Steady State fluorescence spectra, fluorescence lifetime and quantum efficiency of solid film were carried out with FLS980 Spectrometer. Lifetime measurements were carried out by using time-correlated single photon counting method under the excitation of a laser (378.8 nm) with 68.9 ps pulse width.

2.3. Quantum chemical calculations: All the density functional theory (DFT) calculations were carried out under Gaussian 09 (version D.01) package1 on a PowerLeader cluster [44]. The ground-state geometry was fully optimized using DFT with a B3LYP hybrid functional at the basis set level of 6-31G(d, p). The excited-state geometry was optimized by time-dependent density functional theory (TD-DFT) with the Cam-B3LYP functional at the same basis set level. The absorption and emission properties were obtained by using TD-Cam-B3LYP/6-31G(d, p) at the ground state and excited state geometries, respectively. The solvent effect in Hexane were mimicked by using the polarizable continuum model (PCM), in which the equilibrium solvation method was applied for the geometry optimization and the nonequilibrium solvation one was used for the single-point calculation and the excited-state property at the equilibrium geometry.

2.4. Electrochemical characterization: Cyclic voltammetry (CV) was performed with a BAS 100W Bioanalytical Systems, using a glass carbon disk (Φ= 3 mm) as the working electrode, a platinum wire as the auxiliary electrode with a porous ceramic

wick, Ag/Ag^+ as the reference electrode, standardized for the redox couple ferricinium/ferrocene. All solutions were purged with a nitrogen stream for 10 min before measurement. The procedure was performed at room temperature and a nitrogen atmosphere was maintained over the solution during measurements.

2.5. Thermal stability measurements: Thermal gravimetric analysis (TGA) was undertaken on a PerkinElmer thermal analysis system at a heating rate of 10 °C min^{-1} and a nitrogen flow rate of 80 mL min^{-1}. Differential scanning calorimetry (DSC) analysis was carried out using a NETZSCH (DSC-204) instrument at 10 °C min^{-1} while flushing with nitrogen.

2.5. Device fabrication and performances: Glass substrates pre-coated with a 95-nm-thin layer of ITO with a sheet resistance of 20 Ω per square were thoroughly cleaned in an ultrasonic bath of acetone, isopropyl alcohol, detergent, deionized water, and isopropyl alcohol and treated with O_2 plasma for 20 min in sequence. The remaining layers were grown by the thermal evaporation in a high vacuum system with pressure of less than 5×10^{-4} Pa. Electroluminescent (EL) spectra were taken by an optical analyzer, Photo Research PR705. The current density and luminance versus driving voltage (J-V-L) characteristics were measured by Keithley 2420 and Konica Minolta chromameter CS-200, respectively. EQEs were calculated by assuming that the devices were Lambertian light sources. All measurements were carried out at room temperature under ambient conditions without encapsulation except spectra collection.

2.6. Lippert-Mataga model: The influence of solvent environment on the optical property of our compounds can be understood using the Lippert-Mataga equation, a model that describes the interactions between the solvent and the dipole moment of solute:

$$hc(\nu_a-\nu_f) = hc(\nu_a^0-\nu_f^0) - \frac{2(\mu_e-\mu_g)^2}{a^3} f(\varepsilon,n)$$

where f is the orientational polarizability of solvents, μ_e is the dipole moment of excited state, μ_g is the dipole moment of ground state; a is the solvent cavity (Onsager) radius, ε and n are the solvent dielectric and the solvent refractive index, respectively.

2.7. Synthesis

All the reagents and solvents used for the synthesis were purchased from Aldrich or Acros and used as received. All reactions were performed under nitrogen atmosphere. First 4,9-dibromonaphtho[2,3-*c*][1,2,5]thiadiazole (M1) was prepared from the commercially available 1,2-naphthalenediamine in two steps following reported procedures [45].

TPA-NZC was synthesized through sequential Suzuki coupling reactions. The synthesis route is shown in Scheme 1. The structure and purity of TPA-NZC compound are characterized by FT-IR, ^{1}H NMR, ^{13}C NMR, mass spectrometry and elemental analysis.

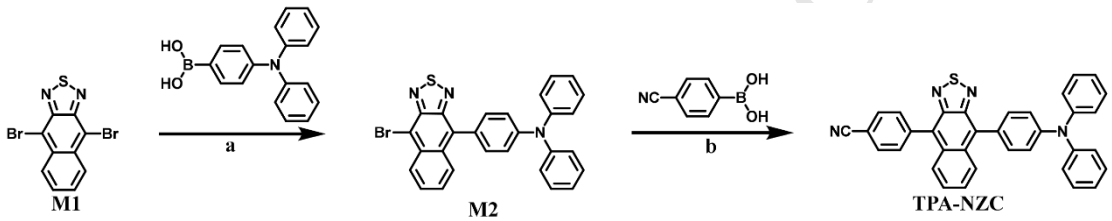

Scheme 1. Synthetic route to TPA-NZC (a. M1, (4-(diphenylamino)phenyl)boronic acid, K_2CO_3, $Pd(PPh_3)_4$, toluene, H_2O, reflux under N_2 at 90 ℃ oil bath for 48 h; b. M2, (4-cyanophenyl)boronic acid, K_2CO_3, $Pd(PPh_3)_4$, toluene, H_2O, C_2H_5OH, reflux under N_2 at 90 ℃ oil bath for 48 h).

Synthesis of 4-(9-bromonaphtho[2,3-c][1,2,5]thiadiazol-4-yl)-N,N-diphenylaniline (M2)

A mixture of M1 (1025 mg, 3 mmol), (4-(diphenylamino)phenyl)boronic (868 mg, 3 mmol), potassium carbonate (3312 mg, 24 mmol), toluene (12 mL) and deionized water (8 mL), with $Pd(PPh_3)_4$ (104 mg, 0.09 mmol) acting as catalyst was refluxed at 90 ˚C for 48 h under nitrogen. After the mixture was cooled down, water (15 mL) was added to the resulting solution and the mixture was extracted with CH_2Cl_2 for several times. The organic phase was dried over Na_2SO_4. After filtration and solvent evaporation, the liquid was purified by chromatography to afford amaranthine solid (M2) (1155 mg, yield ~ 76%). mp: 190-192 ℃. FT-IR (KBr) υ (cm^{-1}): 3439, 3060, 3032, 2927, 2857, 1590, 1508, 1488, 1366, 1329, 1317, 1288, 1268, 1186, 889, 832, 750, 691. MS (ESI): m/z: 507.04. Found: 508.8 $[M+1]^+$. ^{1}H NMR (500 MHz, DMSO)

δ 8.40 (d, J = 9.1 Hz, 1H), 8.06 (d, J = 8.9 Hz, 1H), 7.77 – 7.69 (m, 1H), 7.60 – 7.51 (m, 3H), 7.44 – 7.36 (m, 4H), 7.22 – 7.11 (m, 8H). ^{13}C NMR (126 MHz, $CDCl_3$, δ-ppm) 151.11, 148.12, 147.41, 133.10, 132.49, 132.14, 130.91, 129.47, 128.65, 128.26, 127.73, 127.46, 126.60, 125.28, 123.62, 121.91, 111.02. Elemental analysis. Found: C, 66.02; H, 3.68; N, 8.13, S, 6.42. Calc. for $C_{28}H_{18}N_3SBr$: C, 66.15; H, 3.57; N, 8.26, S, 6.31, Br, 15.72.

Synthesis of 4-(9-(4-(diphenylamino)phenyl)naphtho[2,3-c][1,2,5]thiadiazol-4-yl)benzonitrile (TPA-NZC)

A mixture of M2 (1155 mg, 2.3 mmol), (4-cyanophenyl)boronic acid (441 mg, 3 mmol), potassium carbonate (3312 mg, 24 mmol), toluene (12 mL), absolute alcohol (6 ml) and deionized water (8 mL), with $Pd(PPh_3)_4$ (120 mg, 0.1 mmol) acting as catalyst was refluxed at 90 ˚C for 48 h under nitrogen. After the mixture was cooled down, water (20 mL) was added to the resulting solution and the mixture was extracted with CH_2Cl_2 for several times. The organic phase was dried over Na_2SO_4. After filtration and solvent evaporation, the liquid was purified by chromatography to afford violet solid (TPA-NZC) (787 mg, yield ~ 65%). mp: 260-261 ℃. FT-IR (KBr) υ (cm^{-1}): 3443, 3036, 2222, 1590, 1492, 1509, 1448, 1399, 1330, 1289, 1187, 1024, 890, 833, 764, 698, 621. MS (ESI): m/z: 530.16. Found: 530.29 $[M]^+$. ^{1}H NMR (500 MHz, DMSO, δ-ppm) 8.11 (dd, J = 12.6, 8.6 Hz, 3H), 7.88 (d, J = 8.0 Hz, 2H), 7.86 – 7.79 (m, 1H), 7.58 (d, J = 8.1 Hz, 2H), 7.56 – 7.49 (m, 2H), 7.41 (t, J = 7.7 Hz, 4H), 7.21 (t, J = 8.1 Hz, 6H), 7.15 (t, J = 7.3 Hz, 2H). ^{13}C NMR (126 MHz, $CDCl_3$, δ-ppm) 151.36, 151.01, 148.10, 147.44, 141.65, 132.27, 132.18, 131.93, 131.80, 131.68, 129.47, 129.05, 127.68, 127.30, 127.08, 126.28, 126.03, 125.30, 123.61, 121.96, 118.83, 112.03. Elemental analysis. Found: C, 79.35; H, 4.03; N, 10.69, S, 5.91. Calc. for $C_{35}H_{22}N_4S$: C, 79.22; H, 4.18; N, 10.56; S, 6.04.

3. Results and discussion

3.1. Theoretical analysis

Density functional theory (DFT) was carried out to understand the excited state properties of TPA-NZC using the Gaussian 09 package. The highest occupied molecular orbital (HOMO) is mainly localized on the TPA unit with a small distribution on NZ unit, while the lowest unoccupied molecular orbital (LUMO) is predominantly localized on NZC unit (Figure S1). Thus, the TPA unit acts as donor and NZC unit serves as acceptor in TPA-NZC. For the optimized ground state geometry (Figure 1a), TPA-NZC shows a moderate twist angle of 54° between NZC acceptor and phenyl ring of TPA. As a comparison, the twist angle is further decreased to 39° at the optimized geometry of excited state. The appropriate twist angle facilitates the formation of HLCT excited state with the increased oscillator strength due to the enhanced coupling between donor and acceptor, corresponding to the improved PL efficiency.

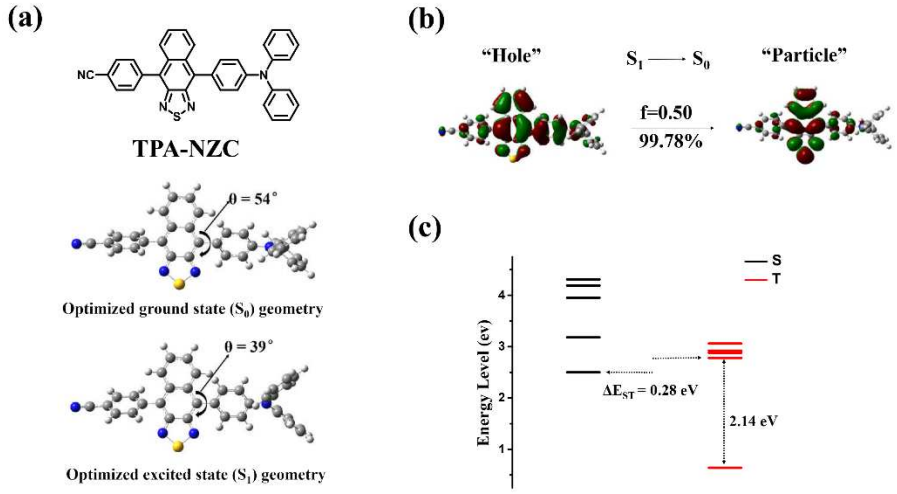

Figure 1. (a) Molecular structure, optimized ground state and excited state geometry of TPA-NZC; (b) NTO for $S_1 \rightarrow S_0$ transition in TPA-NZC. Herein, f represents for the oscillator strength, and the percentage weights of hole-particle are given; (c) Excited state (singlet and triplet) energy level landscape of TPA-NZC at the geometry of S_0 state.

The band gap of TPA-NZC was calculated to be 2.21 eV which was narrower than 2.32 eV of TPA-NZP [27], due to the introduction of cyano group showing the strong electron-withdrawing property. In fact, LUMO energy of TPA-NZC decreases more largely than its HOMO energy, resulting in the decreased band gap of TPA-NZC

relative to that of TPA-NZP (Figure S2). Furthermore, the natural transition orbital (NTO) was performed to analyze the electron transition character of the excited state (Figure 1b and Figure S3). For $S_1 \rightarrow S_0$ transition, the hole is mainly delocalized over the whole molecular skeleton, while the particle is concentrated on NZ unit with partial distribution on cyanophenyl and phenyl ring of TPA. The overlap between hole and particle indicates that the $S_1 \rightarrow S_0$ transition consists of both LE and CT components, which is a typical characteristic of HLCT state. Also, the large oscillator strength (f = 0.50) of TPA-NZC was obtained for $S_1 \rightarrow S_0$ transition, indicating a large radiative transition probability for high PL efficiency.

In the meantime, to confirm a "hot exciton" channel for efficient RISC in TPA-NZC, five singlet states (S_1 to S_5) and five triplet states (T_1 to T_5) were estimated using TD-CAM-B3LYP/6-31G** at the ground state geometry (Figure 1c). A very large energy gap of 2.14 eV was found between T_1 and T_2 state, which is beneficial to slow down the internal conversion rate (k_{IC}) from T_2 to T_1 state according to energy gap law. Moreover, a relatively small energy splitting (ΔE_{ST}) of 0.28 eV is observed between S_1 and T_2 state, so that the RISC process from T_2 to S_1 state can compete with the internal conversion process from T_2 to T_1 state. Such energy level diagram meets the requirement of "hot exciton" mechanism very well, which contributes to high exciton utilization in NIR fluorescent OLEDs. As expected, both high PL efficiency and high exciton utilization may collaborate to realize highly efficient NIR fluorescent OLEDs.

3.2. Photophysical properties

To clarify the photophysical properties of TPA-NZC, the ultraviolet-visible (UV-vis) and PL spectra of TPA-NZC were measured in the different polar solvents and solid state, respectively (Figure 2a, Figure 2b, Figure S4 and Table S1). In the case of tetrahydrofuran (THF) solution, TPA-NZC shows a low-energy absorption band around 505 nm, and a NIR fluorescence emission at 717 nm with high η_{PL} of 21.8%. With the increasing polarity of solvents, the absorption spectra remain almost

unchanged, which indicates that the dipole moment of ground state is quite insensitive to different solvents. On the contrary, the PL spectra of TPA-NZC are significantly red-shifted from 638 nm in low-polarity hexane to 750 nm in high-polarity dichloromethane, together with a gradually broadened full width at half maximum (FWHM), indicating a typical feature of strong CT state. In order to deeply understand the evolution of the excited state with the increase of solvent polarity, the Lippert-Mataga model was used to estimate the dipole moment of the excited state (μ_e). The linear relation of the stokes shift (υ_a-υ_f) against the orientation polarizability f(ε,n) was fitted for TPA-NZC (Figure 2c), which shows two linear-sections in low-polarity and high-polarity region, respectively. As a result, the μ_{es} were estimated to be 11.8 D in low-polarity and 20.7 D in high-polarity, respectively, which indicates that a certain LE state component in low-polarity and CT-dominated state in high-polarity. Thus, the inter-crossing and coexistence between LE and CT components can be expected for excited state (S_1) in medium polarity solvents. Furthermore, the lifetime of excited state in the different polarity solvents was characterized using time-resolved fluorescence (Figure S5). The single-component lifetime was obtained in all polarity solvents (e.g. τ = 7.7 ns in hexane, τ = 5 ns in butyl ether, τ = 4.0 ns in ethyl ether, τ = 3.8 ns in THF, τ = 5 ns in methylene chloride), indicating the typical characteristic of HLCT state in medium polarity solvents, instead of two mixing states. Meanwhile, a high η_{PL} of 21.8% was still maintained for TPA-NZC in medium-polarity THF solvent, especially for the narrow-bandgap NIR emission at 717 nm, which may be ascribed to the formation of HLCT state in medium-polarity. In comparison with UV-vis absorption spectrum in THF solution, the vacuum-evaporated film is significantly red-shifted by 25 nm, which demonstrates a certain degree of intermolecular interaction in solid state. The extracted data of TPA-NZC in the film state are summarized in Table 1. For the PL spectrum of the film, TPA-NZC also shows a NIR emission with maximum wavelength at 710 nm, which is very close to the maximum emission peak (717 nm) in THF solution, indicating that the polarization effect of TPA-NZC in solid state is very similar to that in THF solvent. Moreover, it is noteworthy that TPA-NZC also possesses a single-component lifetime

(τ = 5.1 ns) in the film, which can be attributed to the characteristic of HLCT state in film. Owing to HLCT state characteristic, TPA-NZC also maintains a high PL efficiency (η_{PL} = 17%) in the film.

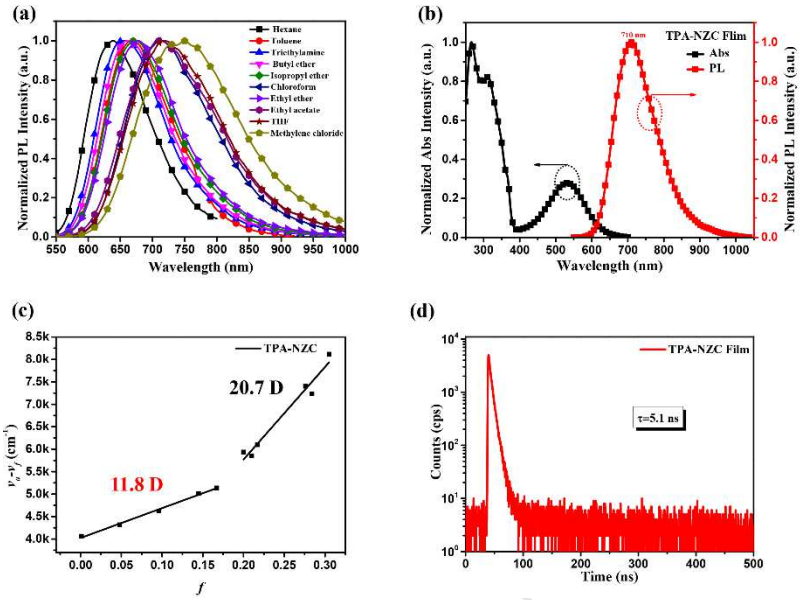

Figure 2. (a) Solvatochromic PL spectra of TPA-NZC with an increasing polarity of solvents; (b) The UV-vis and PL spectra of TPA-NZC under the film state; (c) Linear fitting of Lippert-Mataga model (the solid squares represent the Stokes shifts of TPA-NZC in different solvents); (d) Transient PL decay behaviour of TPA-NZC under the film state.

TPA-NZP without cyano group in D-A molecule which has been reported, just emitted the deep-red fluorescence at the wavelength of 668 nm in film [27]. The introduction of cyano group makes TPA-NZC not only show a largely redshifted emission of 42 nm but also maintain the high PL efficiency relative to those of TPA-NZP.

Moreover, to investigate the influence of the aggregation effects on the fluorescence behavior, The PL spectra of TPA-NZC was measured in THF/water mixtures with different water fractions (f_w) (Figure S17). The pure THF solution (50 × 10^{-6} M) of TPA-NZC emits the NIR light with an emission maximum at 717 nm. With the increase of water ratio (fw$\leqslant$ 50), the emission of TPA-NZC is gradually redshifted accompanied by the rapidly decreasing emission intensity. The phenomenon may be resulted from the twisted intramolecular charge transfer (TICT)

state with the increasing solvent polarity. Once f_w is increased beyond 60%, the emission intensity was significantly increased, demonstrating AIE activity due to the restricted molecular motion [46-48].

Table 1 Photophysical properties and thermal stability of TPA-NZC.

Compound	λ_{abs} [a]	λ_{em} [nm] [b]	η_{PL} [c]	HOMO/LUMO [eV] [d]	Tg/Td [℃]
TPA-NZC	266, 311, 530	710	17%	-5.25/-3.44	110/308

[a] Absorption in a neat film. [b] Emission in a neat film. [c] PL efficiency in a neat film. [d] Determined from cyclic voltammetry.

3.3. Thermal and electrochemical properties

Both thermal and electrochemical properties of emitter are important prerequisites for OLED structure design and fabrication. The differential scanning calorimetry (DSC) and thermogravimetric analysis (TGA) were measured for TPA-NZC. Its glass transition temperature (T_g) and thermal decomposition temperature (T_d) are determined as 110 ℃ and 308 ℃, respectively, indicating the good thermal stability of TPA-NZC (Figure S7). Cyclic voltammetry (CV) was performed in a three-electrode cell setup to obtain the electrochemical properties of TPA-NZC. The HOMO and LUMO energy levels of TPA-NZC are estimated as -5.25 eV and -3.44 eV, according to the onset potentials of the first oxidation wave and the first reduction wave, respectively (Figure S6). Thus, the electrical bandgap of TPA-NZC is obtained as 1.81 eV, which is very close to 1.73 eV of the emission bandgap in THF. Additionally, TPA-NZC exhibits the excellent reversibility of oxidation and reduction processes, implying a good electrochemical stability during the charge injection and charge transport in OLED device.

3.4. Electroluminescence performance

To evaluate the EL performance of NIR material TPA-NZC as an emitter, a non-doped

OLED was firstly fabricated with a multilayer device: ITO/TAPC (40 nm)/TPA-NZC (25 nm) /TmPyPb (55 nm)/LiF (1 nm)/Al (100 nm), where 1,1-bis[(di-4-tolylamino)phenyl]-cyclohexane (TAPC) acted as the hole-transporting layer and 1,3,5-tri(*m*-pyrid-3-yl-phenyl)benzene (TmPyPb) served as the electron-transporting layer. The results of EL performance are recorded in Figure 3c and 3d, including EL spectrum, external quantum efficiency (EQE) versus current density, and current density–voltage–luminance (J–V–L) curves for the device. TPA-NZC device exhibits an excellent NIR emission with EL wavelength at 702 nm, which is nearly the same maximum as that of PL spectrum (710 nm) in evaporated film, and its Commission Internationale de L'Eclairage (CIE) coordinate is obtained as (0.685, 0.299). TPA-NZC device shows a low turn-on voltage (V_{on}) of 3.4 V and a maximum brightness of 757 cd m^{-2}. Eventually, TPA-NZC device harvests a relatively high maximum EQE of 1.2%, which is a valuable one among the high-efficiency non-doped NIR fluorescent OLEDs that have been ever reported. It is worth mentioning that the EQE of TPA-NZC device can still remain as high as 1.09% at high current density of 448 mA cm^{-2}, which suggests that TPA-NZC device has a relatively slow efficiency roll-off as a result of the "hot exciton" and HLCT state mechanism.

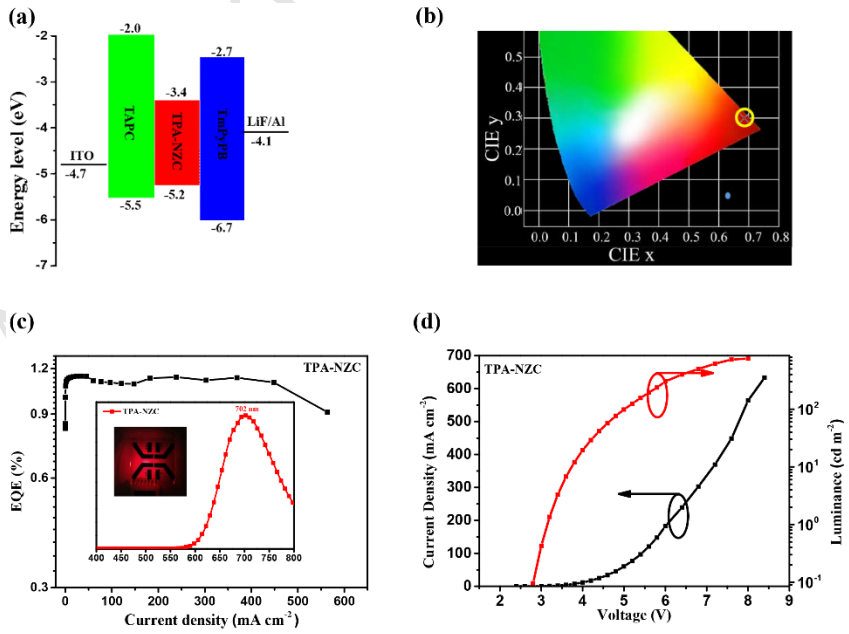

Figure 3. (a) Schematic energy level diagram of TPA-NZC device; (b) CIE coordinate

of TPA-NZC at 1 mA cm^{-2}; (c) EQE-current-density characteristics of non-doped device (the inset graph is the EL spectrum at 1 mA cm^{-2}); (d) Current density-voltage-luminance curves of non-doped device.

Moreover, the theoretical exciton utilization efficiency (η_S) can be roughly evaluated based on the EQE equation of OLED:

$$\eta_{EQE} = \eta_{IQE} \times \eta_{out} = \eta_{rec} \times \eta_{PL} \times \eta_S \times \eta_{out}$$

Where η_{out} is the light out-coupling efficiency ($\eta_{out} \approx 20\%$), η_{rec} is the recombination efficiency of injected holes and electrons ($\eta_{rec} \approx 100\%$), η_S is the exciton utilization efficiency in OLEDs, and η_{PL} is the PL efficiency of the emitter layer ($\eta_{PL} \approx 17\%$). Theoretically, the η_S value is estimated to be 35.2%, which also exceeds the upper limit (25%) of singlet exciton yield in traditional fluorescent materials.

In addition, we also fabricated the doped OLED with the device structure as: ITO/TAPC (40 nm)/EML (25 nm)/TmPyPb (55 nm)/LiF (1 nm)/Al (100 nm), where the emissive layer (EML) is composed of host CBP and dopant of 6 wt% TPA-NZC. The doped OLED exhibits a deep-red emission with the EL spectrum at 656 nm and a CIE coordinate of (0.657, 0.335). The doped device also shows an excellent EL performance, such as a low V_{on} of 3.2 V, the maximum EQE of 3.2% and the maximum brightness of 2237 cd m^{-2}. We have measured the PL efficiency of the doped film. The η_{PL} of the doped film was 37%. Theoretically, the η_S value is estimated to be 43.2%, which also exceeds the upper limit (25%) of singlet exciton yield in traditional fluorescent materials. these details of the doped device are summarized in Figure S8-S11 and Table S2.

4. Conclusion

In summary, the cyanophenyl is used as an ancillary acceptor to further enhance the electron-withdrawing ability of NZ acceptor in a D-A molecule of TPA-NZP, aiming to achieve a high-performance NIR fluorescent material. In this case, the TPA-NZC

was designed and synthesized, which exhibited a more red-shifted NIR emission at λ_{max} = 710 nm with a higher PL efficiency of η_{PL} = 17% in evaporated film in contrast with those of parent TPA-NZP (λ_{max} = 668 nm and η_{PL} = 15%). Interestingly, the introduction of the cyanophenyl results in a large redshift of emission without the sacrifice of η_{PL}, indicating an exception within the framework of the energy gap law. Both quantum chemical calculations and photophysical characterizations suggest that TPA-NZC possesses HLCT state character and "hot exciton" RISC channel, which contribute to a high η_{PL} and high exciton utilization in OLED, respectively. The non-doped OLED of TPA-NZC exhibits a NIR emission at 702 nm with a maximum EQE of 1.2%, while the doped device achieves a deep-red emission at 656 nm with a maximum EQE of 3.2%. These results demonstrate that the cyanophenyl can be used as an ancillary acceptor to construct the narrow-bandgap light-emitting materials with maintenance of PL efficiency in D-A systems, especially for high-efficiency deep-red and NIR fluorescent materials. Also, the HLCT state and "hot exciton" mechanism were further validated to design the new-generation, pure-organic, high-efficiency and low-cost fluorescent OLED materials.

Acknowledgements

This work is supported by the National Natural Science Foundation of China (51473063, 91233116 and 51673083), the National Key Basic Research and Development Program of China (Grant NO. 2016YFB0401001 and 2015CB655003) and the Open Project Foundation of the State Key Laboratory of Luminescence and Applications (Changchun Institute of Optics, Fine Mechanics and Physics of the Chinese Academy of Science, SKLA-2016-04).

References

[1] Sasaki E, Kojima H, Nishimatsu H, Urano Y, Kikuchi K, Hirata Y, et al. Highly sensitive near-infrared fluorescent probes for nitric oxide and their application to isolated organs. J Am Chem Soc. 2005;127(11):3684-3685.

[2] Borek C, Hanson K, Djurovich PI, Thompson ME, Aznavour K, Bau R, et al. Highly Efficient, Near-Infrared Electrophosphorescence from a Pt–Metalloporphyrin Complex. Angew Chem Int Ed. 2007;119(7):1127-1130.

[3] Yuan L, Lin W, Zhao S, Gao W, Chen B, He L, et al. A unique approach to development of near-infrared fluorescent sensors for in vivo imaging. J Am Chem Soc. 2012;134(32):13510-13523.

[4] Qin W, Ding D, Liu J, Yuan WZ, Hu Y, Liu B, et al. Biocompatible Nanoparticles with Aggregation‐Induced Emission Characteristics as Far‐Red/Near‐Infrared Fluorescent Bioprobes for In Vitro and In Vivo Imaging Applications. Adv Funct Mater. 2012;22(4):771-779.

[5] Shao A, Xie Y, Zhu S, Guo Z, Zhu S, Guo J, et al. Far‐Red and Near‐IR AIE‐Active Fluorescent Organic Nanoprobes with Enhanced Tumor‐Targeting Efficacy: Shape‐Specific Effects. Angew Chem Int Ed. 2015;127(25):7383-7388.

[6] S. D. Cummings RE. Tuning the Excited-State Properties of Platinum(II) Diimine Dithiolate Complexes. J Am Chem Soc. 1996;118(118):1949 - 1960.

[7] Ly KT, Chen-Cheng R-W, Lin H-W, Shiau Y-J, Liu S-H, Chou P-T, et al. Near-infrared organic light-emitting diodes with very high external quantum efficiency and radiance. Nature Photonics. 2017;11(1):63-68.

[8] Lee TC, Hung JY, Chi Y, Cheng YM, Lee GH, Chou PT, et al. Rational Design of Charge‐Neutral, Near‐Infrared‐Emitting Osmium (II) Complexes and OLED Fabrication. Adv Funct Mater. 2009;19(16):2639-2647.

[9] Cao X, Miao J, Zhu M, Zhong C, Yang C, Wu H, et al. Near-infrared polymer light-emitting diodes with high efficiency and low efficiency roll-off by using solution-processed iridium (III) phosphors. Chem Mater. 2014;27(1):96-104.

[10] Zhang Q, Li B, Huang S, Nomura H, Tanaka H, Adachi C. Efficient blue organic

light-emitting diodes employing thermally activated delayed fluorescence. Nature Photonics. 2014;8(4):326-332.

[11] Zhang Q, Kuwabara H, Potscavage Jr WJ, Huang S, Hatae Y, Shibata T, et al. Anthraquinone-based intramolecular charge-transfer compounds: computational molecular design, thermally activated delayed fluorescence, and highly efficient red electroluminescence. J Am Chem Soc. 2014;136(52):18070-18081.

[12] Chen D, Wang Z, Wang D, Wu Y-C, Lo C-C, Lien A, et al. Efficient exciplex organic light-emitting diodes with a bipolar acceptor. Org Electron. 2015;25:79-84.

[13] Chen D, Xie G, Cai X, Liu M, Cao Y, Su SJ. Fluorescent Organic Planar pn Heterojunction Light‐Emitting Diodes with Simplified Structure, Extremely Low Driving Voltage, and High Efficiency. Adv Mater. 2016;28(2):239-244.

[14] Xie G, Li X, Chen D, Wang Z, Cai X, Chen D, et al. Evaporation‐and Solution‐Process‐Feasible Highly Efficient Thianthrene‐9, 9′, 10, 10′‐Tetraoxide‐Based Thermally Activated Delayed Fluorescence Emitters with Reduced Efficiency Roll‐Off. Adv Mater. 2016;28(1):181-187.

[15] Wang S, Yan X, Cheng Z, Zhang H, Liu Y, Wang Y. Highly Efficient Near‐Infrared Delayed Fluorescence Organic Light Emitting Diodes Using a Phenanthrene‐Based Charge‐Transfer Compound. Angew Chem Int Ed. 2015;54(44):13068-13072.

[16] Yuan Y, Hu Y, Zhang YX, Lin JD, Wang YK, Jiang ZQ, et al. Over 10% EQE Near‐Infrared Electroluminescence Based on a Thermally Activated Delayed Fluorescence Emitter. Adv Funct Mater. 2017.

[17] Yamanaka T, Nakanotani H, Hara S, Hirohata T, Adachi C. Near-infrared organic light-emitting diodes for biosensing with high operating stability. Appl Phys Express. 2017;10(7):074101.

[18] Lee J, Shizu K, Tanaka H, Nomura H, Yasuda T, Adachi C. Oxadiazole-and triazole-based highly-efficient thermally activated delayed fluorescence emitters for organic light-emitting diodes. J Mater Chem C. 2013;1(30):4599-604.

[19] Cai M, Zhang D, Huang T, Song X, Duan L. Multifunctional Materials for High-Performance Double-Layer Organic Light-Emitting Diodes: Comparison of Isomers with and without Thermally Activated Delayed Fluorescence. ACS Appl Mater Interfaces.

2017;9(20), 17279-17289.

[20] Zhang D, Duan L, Li C, Li Y, Li H, Zhang D, et al. High‐Efficiency Fluorescent Organic Light‐Emitting Devices Using Sensitizing Hosts with a Small Singlet−Triplet Exchange Energy. Adv Mater. 2014;26(29):5050-5055.

[21] Zhang D, Duan L, Zhang Y, Cai M, Zhang D, Qiu Y. Highly efficient hybrid warm white organic light-emitting diodes using a blue thermally activated delayed fluorescence emitter: exploiting the external heavy-atom effect. Light: Science and Applications. 2015;4(1):e232.

[22] Zhang D, Zhao C, Zhang Y, Song X, Wei P, Cai M, et al. Highly Efficient Full-Color Thermally Activated Delayed Fluorescent Organic Light-Emitting Diodes: Extremely Low Efficiency Roll-Off Utilizing a Host with Small Singlet–Triplet Splitting. ACS Appl Mater Interfaces. 2017;9(5):4769-4777.

[23] Liu XK, Chen Z, Qing J, Zhang WJ, Wu B, Tam HL, et al. Remanagement of Singlet and Triplet Excitons in Single‐Emissive‐Layer Hybrid White Organic Light‐Emitting Devices Using Thermally Activated Delayed Fluorescent Blue Exciplex. Adv Mater. 2015;27(44):7079-85.

[24] Chiang CJ, Kimyonok A, Etherington MK, Griffiths GC, Jankus V, Turksoy F, et al. Ultrahigh Efficiency Fluorescent Single and Bi‐Layer Organic Light Emitting Diodes: The Key Role of Triplet Fusion. Adv Funct Mater. 2013;23(6):739-46.

[25] Xue J, Li C, Xin L, Duan L, Qiao J. High-efficiency and low efficiency roll-off near-infrared fluorescent OLEDs through triplet fusion. Chem Sci. 2016;7(4):2888-95.

[26] Yao L, Zhang S, Wang R, Li W, Shen F, Yang B, et al. Highly Efficient Near‐Infrared Organic Light‐Emitting Diode Based on a Butterfly-Shaped Donor-Acceptor Chromophore with Strong Solid-State Fluorescence and a Large Proportion of Radiative Excitons. Angew Chem Int Ed. 2014;126(8):2151-5.

[27] Li W, Pan Y, Yao L, Liu H, Zhang S, Wang C, et al. A Hybridized Local and Charge-Transfer Excited State for Highly Efficient Fluorescent OLEDs: Molecular Design, Spectral Character, and Full Exciton Utilization. Adv Opt Mater. 2014;2(9):892-901.

[28] Liu H, Bai Q, Yao L, Zhang H, Xu H, Zhang S, et al. Highly efficient near ultraviolet organic light-emitting diode based on a meta-linked donor–acceptor molecule. Chem Sci. 2015;6(7):3797-804.

[29] Wang C, Li X, Pan Y, Zhang S, Yao L, Bai Q, et al. Highly Efficient Nondoped Green Organic Light-Emitting Diodes with Combination of High Photoluminescence and High Exciton Utilization. ACS Appl Mater Interfaces. 2016;8(5):3041-9.

[30] Yao L, Pan Y, Tang X, Bai Q, Shen F, Li F, et al. Tailoring Excited-State Properties and Electroluminescence Performance of Donor–Acceptor Molecules through Tuning the Energy Level of the Charge-Transfer State. J Phys Chem C. 2015;119(31):17800-8.

[31] Liu H, Bai Q, Li W, Guo Y, Yao L, Gao Y, et al. Efficient deep-blue non-doped organic light-emitting diode with improved roll-off of efficiency based on hybrid local and charge-transfer excited state. RSC Adv. 2016;6(74):70085-90.

[32] Gao Y, Zhang S, Pan Y, Yao L, Liu H, Guo Y, et al. Hybridization and de-hybridization between the locally-excited (LE) state and the charge-transfer (CT) state: a combined experimental and theoretical study. Phys Chem Chem Phys. 2016;18(35):24176-84.

[33] Zhou C, Zhang T, Zhang S, Liu H, Gao Y, Su Q, et al. Isomerization effect of triphenylamine-acridine derivatives on excited-state modification, photophysical property and electroluminescence performance. Dyes Pigments. 2017;146:558-66.

[34] Liu T, Zhu L, Gong S, Zhong C, Xie G, Mao E, et al. A Red Fluorescent Emitter with a Simultaneous Hybrid Local and Charge Transfer Excited State and Aggregation-Induced Emission for High-Efficiency, Low Efficiency Roll-Off OLEDs. Adv Opt Mater. 2017;5(13):1700145.

[35] Yuan Y, Chen J-X, Lu F, Tong Q-X, Yang Q-D, Mo H-W, et al. Bipolar Phenanthroimidazole Derivatives Containing Bulky Polyaromatic Hydrocarbons for Nondoped Blue Electroluminescence Devices with High Efficiency and Low Efficiency Roll-Off. Chem Mater. 2013;25(24):4957-65.

[36] Pan Y, Li W, Zhang S, Yao L, Gu C, Xu H, et al. High Yields of Singlet Excitons in Organic Electroluminescence through Two Paths of Cold and Hot Excitons. Adv Opt Mater. 2014;2(6):510-5.

[37] Li W, Pan Y, Xiao R, Peng Q, Zhang S, Ma D, et al. Employing ~100% Excitons in OLEDs by Utilizing a Fluorescent Molecule with Hybridized Local and Charge-Transfer Excited State. Adv Funct Mater. 2014;24(11):1609-14.

[38] Liu T, Zhu L, Zhong C, Xie G, Gong S, Fang J, et al. Naphthothiadiazole‐Based

Near‐Infrared Emitter with a Photoluminescence Quantum Yield of 60% in Neat Film and External Quantum Efficiencies of up to 3.9% in Nondoped OLEDs. Adv Funct Mater. 2017;27(12).

[39] Wang C, Li XL, Gao Y, Wang L, Zhang S, Zhao L, et al. Efficient Near‐Infrared (NIR) Organic Light‐Emitting Diodes Based on Donor-Acceptor Architecture: An Improved Emissive State from Mixing to Hybridization. Adv Opt Mater. 2017;DOI: 10.1002/adom.201700441.

[40] Uoyama H, Goushi K, Shizu K, Nomura H, Adachi C. Highly efficient organic light-emitting diodes from delayed fluorescence. Nature. 2012;492(7428):234-8.

[41] Zhang S, Li W, Yao L, Pan Y, Shen F, Xiao R, et al. Enhanced proportion of radiative excitons in non-doped electro-fluorescence generated from an imidazole derivative with an orthogonal donor-acceptor structure. Chem Commun. 2013;49(96):11302-4.

[42] Zhang S, Yao L, Peng Q, Li W, Pan Y, Xiao R, et al. Achieving a Significantly Increased Efficiency in Nondoped Pure Blue Fluorescent OLED: A Quasi-Equivalent Hybridized Excited State. Adv Funct Mater. 2015;25(11):1755-1762.

[43] Zhang S, Dai Y, Luo S, Gao Y, Gao N, Wang K, et al. Rehybridization of Nitrogen Atom Induced Photoluminescence Enhancement under Pressure Stimulation. Adv Funct Mater. 2017;27(1):1602276.

[44] Frisch M. J, Trucks G. W, Schlegel H. B, Scuseria G. E, Robb M. A, Cheeseman J. R, Scalmani G, Barone V, Mennucci B, Petersson G. A, Nakatsuji H, Caricato M, H X. Li. Hratchian P, Izmaylov A. F, Bloino J, Zheng G, Sonnenberg J. L, Hada M, Ehara M, Toyota K, Fukuda R, Hasegawa J, Ishida M, Nakajima T, Honda Y, Kitao O, Nakai H, Vreven T, Montgomery J.A, Peralta J. E, Ogliaro F, Bearpark M, Heyd J. J, Brothers E, Kudin K. N, Staroverov V. N, Kobayashi R, Normand J, Raghavachari K, Rendell A, Burant J. C, Iyengar S. S, Tomasi J, Cossi M, Rega N, Millam J. M, Klene M, Knox J. E, Cross J. B, Bakken V, Adamo C, Jaramillo J, Gomperts R, Stratmann R. E, Yazyev O, Austin A. J, Cammi R, Pomelli C, Ochterski J. W, Martin R. L, Morokuma K, Zakrzewski V. G, Voth G. A, Salvador P, Dannenberg J. J, Dapprich S, Daniels A. D, Farkas Ö, Foresman J. B, Ortiz J. V, Cioslowski J and Fox D. J, Gaussian 09, Revision D.01,Gaussian, Inc.: Wallingford CT, USA2009.

[45] Wei P, Duan L, Zhang D, Qiao J, Wang L, Wang R, et al. A new type of light-emitting

545 naphtho[2,3-*c*][1,2,5]thiadiazole derivatives: synthesis, photophysical characterization and
546 transporting properties. J Mater Chem. 2008;18(7):806.
547 [46] Qin W, Li K, Feng G, Li M, Yang Z, Liu B, et al. Bright and Photostable Organic
548 Fluorescent Dots with Aggregation-Induced Emission Characteristics for Noninvasive
549 Long-Term Cell Imaging. Adv Funct Mater. 2014;24(5):635-43.
550 [47] Mei J, Hong Y, Lam JW, Qin A, Tang Y, Tang BZ. Aggregation-induced emission: the
551 whole is more brilliant than the parts. Adv Mater. 2014;26(31):5429-79.
552 [48] Chang Z-F, Jing L-M, Chen B, Zhang M, Cai X, Liu J-J, et al. Rational design of
553 asymmetric red fluorescent probes for live cell imaging with high AIE effects and large
554 two-photon absorption cross sections using tunable terminal groups. Chem Sci.
555 2016;7(7):4527-36.

Highlights

1. Cyanophenyl as an ancillary acceptor is attached to Naphtho[2,3-c][1,2,5]thiadiazole for a highly efficient NIR material (TPA-NZC).
2. Experimental and theoretical results demonstrate the “hot exciton” and HLCT characteristic of TPA-NZC molecule.
3. TPA-NZC exhibits a NIR emission at λ_{max} = 710 nm with a high PL efficiency of η_{PL} = 17% in evaporated film.
4. The non-doped device based on TPA-NZC as emitter exhibits a NIR emission at 702 nm with a maximum EQE of 1.2%, and the doped device achieves a deep-red emission at 656 nm with a maximum EQE of 3.2%.